THE JOURNAL OF
PHYSICAL CHEMISTRY
LETTERS
A JOURNAL OF THE AMERICAN CHEMICAL SOCIETY

Nonequilibrium Thermodynamics of Charge Separation in Organic Solar Cells

Waldemar Kaiser, Veljko Janković, Nenad Vukmirović, and Alessio Gagliardi*

Cite This: J. Phys. Chem. Lett. 2021, 12, 6389−6397

Read Online

ACCESS | Metrics & More | Article Recommendations | SI Supporting Information

ABSTRACT: This work presents a novel theoretical description of the nonequilibrium thermodynamics of charge separation in organic solar cells (OSCs). Using stochastic thermodynamics, we take realistic state populations derived from the phonon-assisted dynamics of electron−hole pairs within photoexcited organic bilayers to connect the kinetics with the free energy profile of charge separation. Hereby, we quantify for the first time the difference between nonequilibrium and equilibrium free energy profile. We analyze the impact of energetic disorder and delocalization on free energy, average energy, and entropy. For a high disorder, the free energy profile is well-described as equilibrated. We observe significant deviations from equilibrium for delocalized electron−hole pairs at a small disorder, implying that charge separation in efficient OSCs proceeds via a cold but nonequilibrated pathway. Both a large Gibbs entropy and large initial electron−hole distance provide an efficient charge separation, while a decrease in the free energy barrier does not necessarily enhance charge separation.

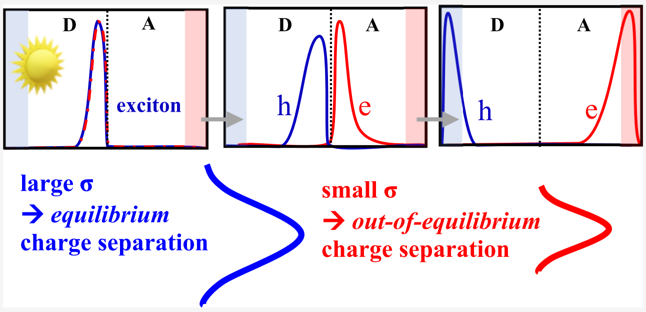

Despite years of research on the fundamental properties of organic solar cells (OSCs), one of the essential aspects of these materials is still under debate: what causes the efficient dissociation of charge transfer (CT) states into free charge carriers despite the presence of the strong Coulomb attraction? Various mechanisms have been proposed to promote the CT separation. On the one hand, "hot" CT states are considered to provide sufficient excess energy for the charges to overcome the binding energy before they relax and become trapped at the bottom of the CT manifold.[1−4] On the other hand, the internal quantum efficiency that is independent of the excitation energy suggests an efficient separation of "cold" CT states.[5,6] The precise mechanism of cold charge separation, however, is to be established.

Kinetic models of charge separation suggest that delocalized charges can efficiently escape their strong binding due to a reduced Coulomb interaction.[7−13] Furthermore, a moderate disorder in combination with delocalization positively impacts charge separation,[10,14] while a strong disorder hampers charge transport,[15,16] traps charge carriers, and influences charge recombination.[17] Thermodynamic considerations reassessed the widespread view that charges have to overcome large energy barriers to become fully separated.[18−22] In materials of higher dimensionality, entropy, reflecting the number of available states, significantly reduces the free energy barrier.[18,21,22] Hood and Kassal emphasized that relying only on dimensionality underestimates the contribution of the energetic disorder, σ, to the free energy for disordered organic semiconductors.[19] Assuming the canonical distribution of CT states in energy, they predict a reduction in free energy barrier with increased σ. For $\sigma \geq 100$ meV, equilibrium thermodynamic arguments suggest that charges are not bound and can be separated under favorable kinetic conditions. The extension of the formalism to include charge delocalization[23] revealed that the positive impact of delocalization on charge separation cannot be rationalized in terms of equilibrium thermodynamics alone, as it predicts an increase in the energy barrier for more delocalized carriers. The conclusions drawn from existing thermodynamic studies of charge separation in OSCs seem to contradict the intuitive picture emerging from kinetic models.

Some of the weaknesses of existing thermodynamic arguments and their possible solutions are as follows: (i) The population of CT states described by the canonical distribution is unrealistic. Nonequilibrated electron−hole pairs due to an incomplete thermalization were indeed observed in CT electroluminescence[24] and photoluminescence[25] measurements in bulk heterojunction OSCs. Giazitzidis et al.[26] proposed to correct the equilibrium free energy with the probability distribution of finding a CT state at a certain distance. Shi et al. emphasize that the disorder-enhanced

Received: June 8, 2021
Accepted: July 2, 2021

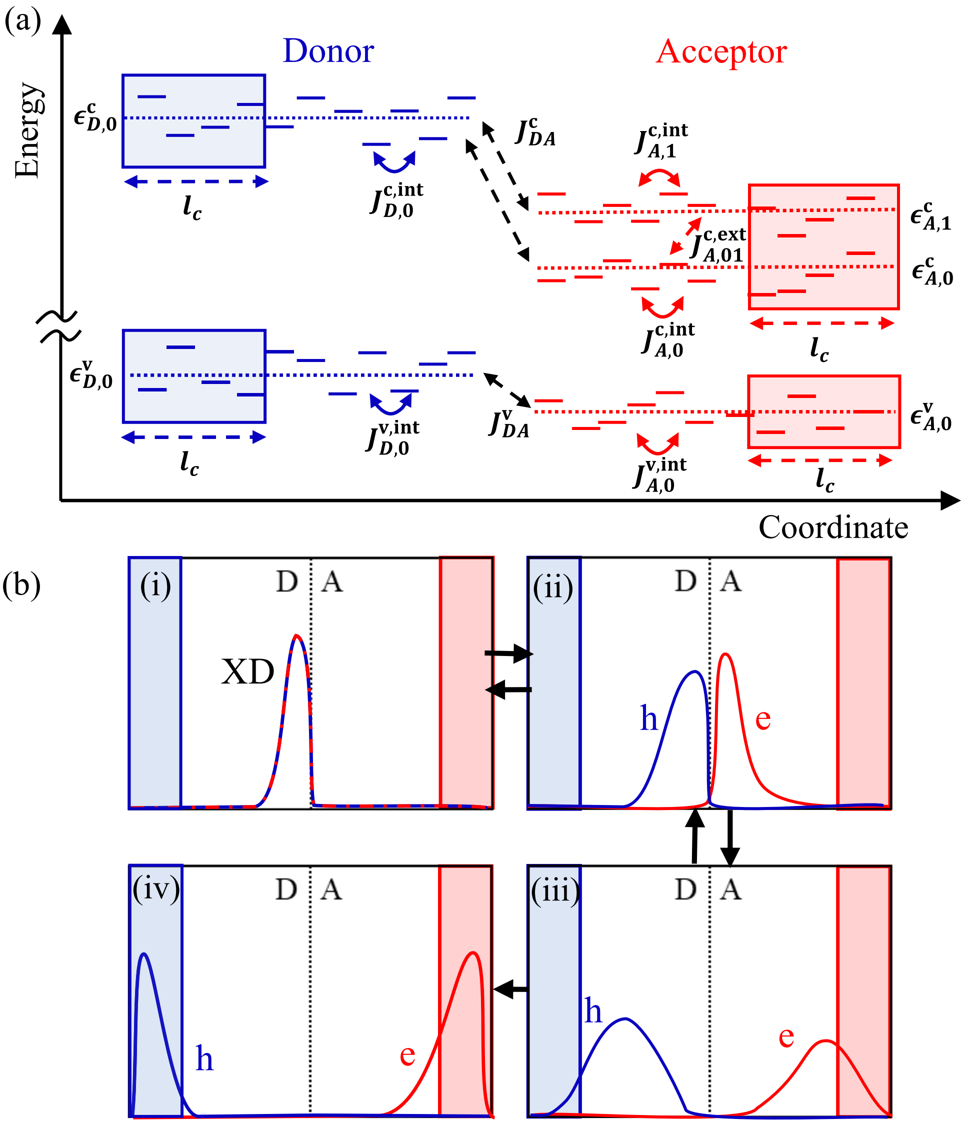

Figure 1. (a) Schematic representation of the organic bilayer model. Dotted lines give the different average on-site energies of the LUMO (superscript c) and of the HOMO (superscript v) in the donor (D) and in the acceptor (A); solid lines represent the actual on-site energies, which vary from the average on-site energies due to the Gaussian energetic disorder σ. The different transfer integrals within the donor ($J_{D,0}^{c/v,int}$) and the acceptor ($J_{A,0/1}^{c/v,int}$) as well as the coupling between the donor and acceptor ($J_{DA}^{c/v}$) are highlighted. In the acceptor region, LUMO (subscript 0) and LUMO+1 (subscript 1) are considered with the transfer integral $J_{A,01}^{ext}$ representing the coupling of the LUMO and LUMO+1 orbitals. Highlighted regions at the left and the right end of the donor and acceptor, respectively, with length l_c visualize contact regions. (b) Representative evolution of an electron–hole pair in the organic bilayer: (i) donor exciton (XD), (ii) CT state—electron in the acceptor and hole in the donor localized at the donor/acceptor interface, (iii) CT state featuring larger intrapair separation and more delocalized carriers, (iv) contact state—electron and hole located in the contact region.

dissociation is a nonequilibrium effect.[14] They observed a deviation of the actual energy barrier from the equilibrium one by averaging Monte Carlo trajectories but neglected the weighting of the energies by their population probability. (ii) The finite lifetime of CT states, which may eliminate a large percentage of possible separation pathways, is completely neglected in previous thermodynamic studies.[18,19,23] (iii) Most of the thermodynamic considerations do not include the coupling of electronic excitations to phonons. Such effects were partially included in previous equilibrium thermodynamic studies in refs 27 and 28.

Previous works gave clear suggestions that the equilibrium free energy profile might not be adequate to study the charge separation process. In this work, we make use of the nonequilibrium free energy rigorously derived from the theory of stochastic thermodynamics[29,30] to connect the kinetic and thermodynamic perspectives on charge separation and quantify for the first time the difference between nonequilibrium and equilibrium free energy. We perform the study for different values of energetic disorder and delocalization and find that this difference is strongest when charge separation efficiency is largest. Our results therefore imply that charge separation in efficient OSCs proceeds via cold, but nonequilibrium, pathways.

To establish the connection between kinetic and thermodynamic properties in the charge separation process in a photoexcited organic bilayer, representing the donor/acceptor interface in OSCs, we use the following procedure: (i) We model the organic bilayer using a minimal microscopic Hamiltonian that captures all important physical effects—

https://doi.org/10.1021/acs.jpclett.1c01817
J. Phys. Chem. Lett. 2021, 12, 6389−6397

delocalization, disorder, electron−hole interaction, and electron−phonon coupling—in the system. We obtain the eigenstates of this Hamiltonian that we classify as states of excitons in the donor, CT states, and contact states; (ii) We compute the transition rates between pairs of states obtained in step (i) and solve the master equation to obtain the nonequilibrium steady-state populations of all non-contact states; (iii) We evaluate the nonequilibrium free energy profile of CT states.

(i) The organic bilayer model used in this step has been reported in previous publications.[10,31] Here, we outline its most important ingredients, while we provide all details in the Supporting Information (section Model Hamiltonian therein). We consider a lattice model with N sites corresponding to the donor material and N sites corresponding to the acceptor material, schematically shown in Figure 1a. The effects of delocalization are included through electronic couplings between neighboring sites, while the effects of disorder are included through random on-site electron and hole energies drawn from Gaussian distributions of standard deviation σ centered around the site energies. An attractive electron−hole interaction is approximated using the Ohno potential. The model parameters were chosen such that the band offsets, band gaps, bandwidths, and binding energies of the donor, acceptor, and CT excitons correspond to the values for the P3HT/PCBM interface. We then solve the eigenvalue problem of this Hamiltonian, which provides a set of excitonic states. On the basis of the spatial distribution of the electron and of the hole component of the excitonic state, we classify these states as (a) donor exciton states—states where both the electron and the hole are predominantly located in the donor, (b) CT states—states where the hole and the electron are located predominantly in the donor and in the acceptor, respectively, and (c) contact states—states where the electron is predominantly located in the region of length l_{c} far away from the interface in the acceptor, while the hole is predominantly located in such a region in the donor (see Figure 1b). Contact states can be considered as states of fully separated charges. A typical spatial distribution of donor, CT, and contact states is shown in Figure 1b. All values of the model parameters are summarized in Table S1, Supporting Information.

(ii) In this step we calculate the steady-state populations f_x^{st} of the excitonic states $|x\rangle$ by solving the master equation

$$0 = g_x - \tau_x^{-1} f_x^{\mathrm{st}} - \sum_{x',x} w_{x'x} f_x^{\mathrm{st}} + \sum_{x' \notin C} w_{xx'} f_{x'}^{\mathrm{st}} \qquad (1)$$

where $w_{x'x}$ is the transition rate from state $|x\rangle$ to state $|x'\rangle$, τ_x is the lifetime of the state $|x\rangle$, and g_x is the generation rate in state $|x\rangle$ that is chosen to mimic the excitation by incident sunlight. The last sum in eq 1 does not include contact states C, because we impose that once a contact state is reached, the charges are fully separated and cannot return back to the system. The detailed models used for phonon-assisted transition rates $w_{x'x}$, lifetimes τ_x, and generation rates g_x are provided in Supporting Information (section Model Hamiltonian therein).

Electron−hole pairs evolve within a phase space of excitonic states with a large energetic disorder and variable mean distance between the wave function of the electron and the hole; see Figure 1b. We assume that the charge separation starts from states of donor excitons (Figure 1b(i)) that are populated as a result of the absorption of natural sunlight. It proceeds via phonon-assisted transitions between space-separated CT states (Figure 1b(ii,iii)) and finishes once the charges are collected at a contact state (Figure 1b(iv)) or recombine. The expression for the charge separation efficiency

$$\eta = \frac{\sum_{x'\in C}\sum_{x\notin C} w_{x'x} f_x^{0}}{\sum_{x\notin C} g_x} \qquad (2)$$

contains phonon-assisted transition rates $w_{x'x}$ toward contact states $|x'\rangle \in C$, which are appreciable only when state $|x\rangle$ features the electron in the acceptor and the hole in the donor part of the bilayer. In the following, instead of considering the full distribution, we concentrate on the steady-state populations of CT states, in which the charges are spatially separated and reside in different regions of the bilayer, as contact states can only be reached when $|x\rangle$ (eq 2) is a CT state.

(iii) The theory of stochastic thermodynamics extends equilibrium thermodynamic concepts to describe thermodynamic quantities of out-of-equilibrium systems and processes that are governed by Markovian dynamics. The major advantages of stochastic thermodynamics are that it can be applied to small-scale systems to study the effect of fluctuations[29,30,32,33] and that it is not restricted to near-equilibrium dynamics.[29,30] Stochastic thermodynamics formulates the first and second laws of thermodynamics for a system that is described by discrete microstates m of energy E_m with probability $p_m(t)$ of the system being in state m. This allows us to define thermodynamic quantities such as the energy of the system, $E = \sum_m p_m E_m$, and the Gibbs entropy, $S = -k_{\mathrm{B}} \sum_m p_m \ln p_m$, from the probability distributions as known from statistical mechanics, with the major difference being that p_m can be time-dependent and out-of-equilibrium. While classical thermodynamics provides fundamental boundaries for entropy production ($\Delta S \geq 0$, second law of thermodynamics), stochastic thermodynamics can quantify the amount of entropy that is produced and even the entropy contribution of each microscopic state transition.[29] Stochastic thermodynamics was used to derive thermodynamic efficiency limits of nanothermoelectric engines at the maximum power point[34] and to derive protocols to extract the maximum work from nanoscale processes,[35] to mention a few examples. An application of stochastic thermodynamics to existing few-level photovoltaic models[36−38] may yield thermodynamic quantities from kinetics but cannot capture the broad CT manifold in terms of energy, delocalization, and electron−phonon coupling. Therefore, a combination of our model and stochastic thermodynamics provides a minimal, yet physically plausible, framework to study the nonequilibrium thermodynamics of charge separation.

Previous equilibrium studies[19,23] assumed the Maxwell−Boltzmann distribution of CT states $|m\rangle$, $f_m^{\mathrm{eq}} \propto e^{-\beta E_m}$, where E_m is the energy of CT state $|m\rangle$, while $\beta = (k_{\mathrm{B}}T)^{-1}$, with T being the phonon-bath temperature. To study if, and to which extent, charge separation occurs out-of-equilibrium, we formulate the free energy F^{st} in the steady state as a function of the intrapair distance r using the free energy relation from stochastic thermodynamics[29,39]

$$\begin{aligned}\beta(F^{\mathrm{st}}(r) - F^{\mathrm{eq}}(r)) &= D_{\mathrm{KL}}(p^{\mathrm{st}} \| p^{\mathrm{eq}}) \\ &= \sum_m p_m^{\mathrm{st}}(r) \ln\left(\frac{p_m^{\mathrm{st}}(r)}{p_m^{\mathrm{eq}}(r)}\right)\end{aligned} \qquad (3)$$

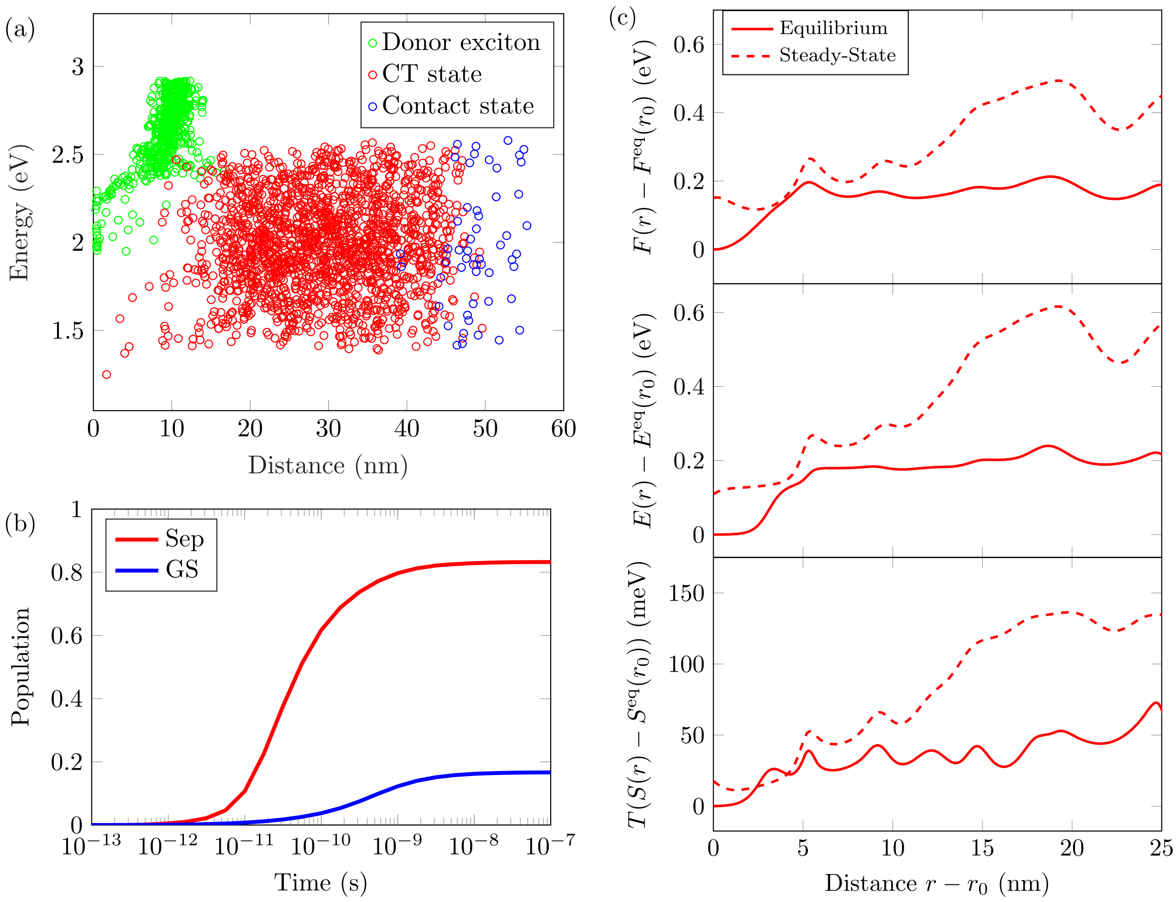

Figure 2. (a) Exemplary distribution of electron−hole pairs in the distance−energy phase space: donor excitons (green), CT states (red), and contact states (blue). (b) Time dependence of fully separated (Sep) and recombined states (GS) for the given network. (c) Distance dependence of the free energy $F(r)$, energy $E(r)$, and entropy contribution $TS(r)$. Solid lines represent the equilibrium values; dashed lines give the nonequilibrium results. All curves are normalized to the equilibrium value (subscript eq) at the distance r_0.

with the Kullback−Leibler (KL) divergence $D_{KL}(p^{st} \| p^{eq})$ between the steady-state probability distribution p^{st} and the equilibrium probability distribution p^{eq} of all CT states $|m\rangle$. For a given r value, the steady-state probability distribution p_m^{st} is obtained from the stationary populations f_m^{st} as follows

$$p_m^{st}(r) = f_m^{st} \times \exp\left(-\frac{(r_m - r)^2}{2{\sigma_b}^2}\right) \left[\sum_k f_k^{st} \times \exp\left(-\frac{(r_k - r)^2}{2{\sigma_b}^2}\right)\right]^{-1} \qquad (4)$$

At the same time, the equilibrium distribution p_m^{eq} is obtained using the approach of Hood and Kassal.[19]

$$p_m^{eq}(r) = \exp(-\beta E_m) \times \exp\left(-\frac{(r_m - r)^2}{2{\sigma_b}^2}\right) \left[\sum_k \exp(-\beta E_k) \times \exp\left(-\frac{(r_k - r)^2}{2{\sigma_b}^2}\right)\right]^{-1} \qquad (5)$$

The KL divergence in eq 3 defines a measure of the difference of a given probability distribution—in our case p^{st}—from a reference probability distribution—here p^{eq}. Note that $D_{KL} \geq 0$ and that D_{KL} takes zero if and only if $p_m^{st} = p_m^{eq}$ for each individual CT state $|m\rangle$. If $p_m^{st} \neq p_m^{eq}$, the CT state $|m\rangle$ is not equilibrated, and consequently $F^{st} > F^{eq}$. The difference between F^{st} and F^{eq} gives us a measure of how close to equilibrium charge separation occurs. This allows us to connect the kinetics of charge separation, given by p^{st}, with thermodynamic quantities of the charge separation process.

Rearranging eq 3 gives the well-known expression of the free energy

$$\begin{aligned} F^{st}(r) &= \sum_m p_m^{st}(r) E_m + \beta^{-1} p_m^{st}(r) \ln p_m^{st}(r) \\ &= E^{st}(r) - TS^{st}(r) \end{aligned} \qquad (6)$$

Using p^{st}, we calculate the average energy $E^{st}(r)$, which electron−hole pairs pass during separation, and the Gibbs entropy $S^{st}(r)$, which accounts for the accessible states.

Note that, in comparison to previous studies,[18,19,23] we replaced the counting of the states within a shell of thickness b by a Gaussian multiplier with width σ_b, accounting for the proximity of CT state $|m\rangle$ to r, to avoid discontinuities in the thermodynamic quantities. In the following, we take $\sigma_b = 0.5$ nm. A sensitivity analysis of σ_b is provided in Figure S4, Supporting Information. We consider the system in the linear regime, where occupations of all states are proportional to the intensity of the incident radiation; the thermodynamic quantities do not depend in this regime on the intensity of incident radiation. This can be straightforwardly proved using eqs 2, 4, 5, and 6.

https://doi.org/10.1021/acs.jpclett.1c01817
J. Phys. Chem. Lett. 2021, 12, 6389−6397

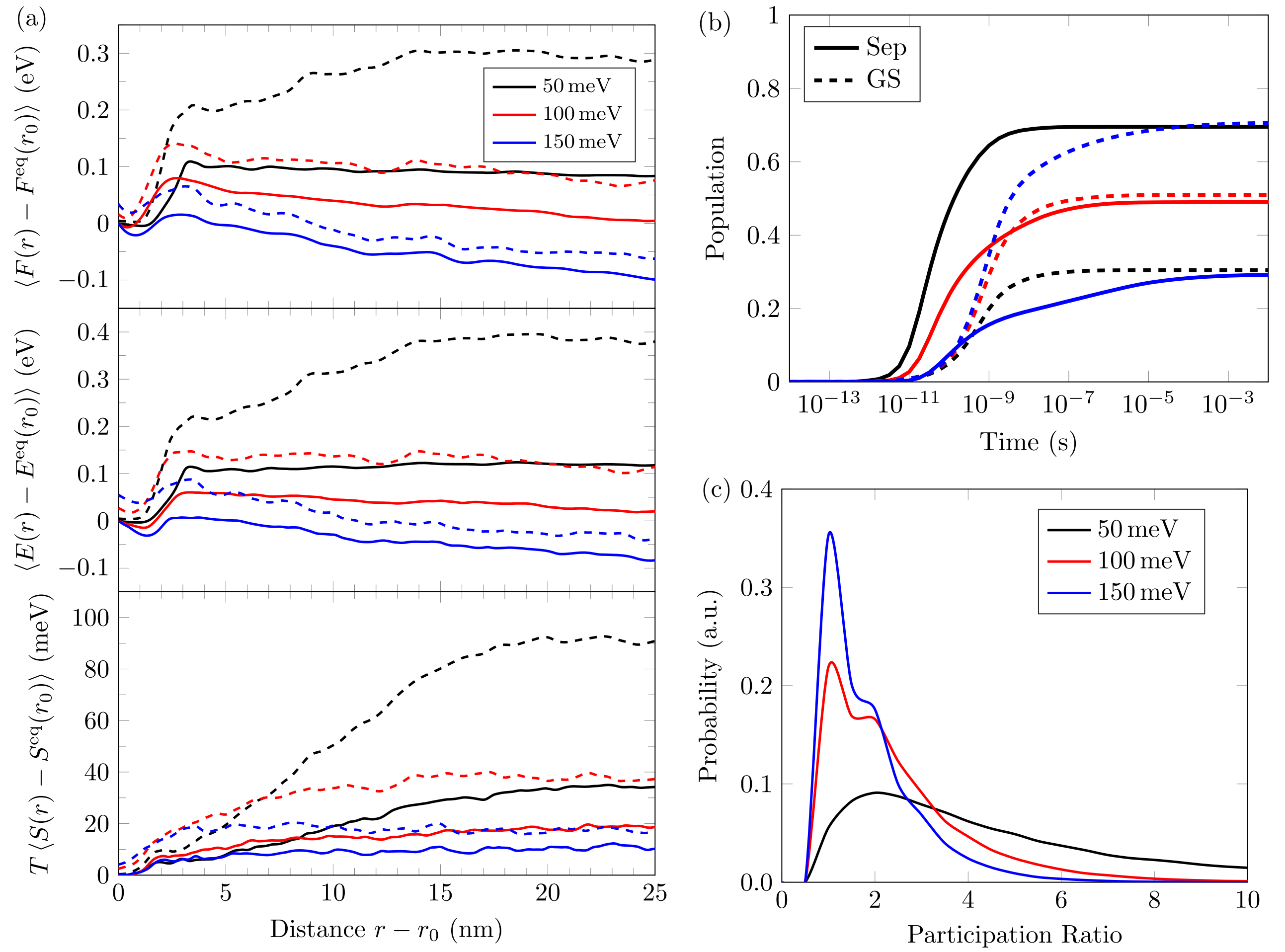

Figure 3. (a) Distance dependence of the free energy $F(r)$, energy $E(r)$, and entropic contribution $TS(r)$ for different disorder σ: 50 meV (black), 100 meV (red), and 150 meV (blue). The $\langle\cdot\rangle$ labels the ensemble average over 256 configurations. r_0 gives the smallest distance of CT states in each configuration. Solid and dashed curves present the equilibrium and stationary thermodynamic quantities, respectively. All curves are normalized to the equilibrium value (superscript eq) at the distance r_0. (b) Time dependence of the separation yield (solid line) and the recombined states (dashed line). (c) Distribution of CT states as a function of their electron participation ratio. All curves in (a−c) show averages across 256 configurations.

First, we present the capabilities of the developed method by calculating the free energy for a particular network of exciton states at σ = 50 meV. Figure 2a shows the energy and the intrapair distance of each electron−hole pair (donor excitons, CT states, and contact states). The time evolution of fully separated and of recombined electron−hole pairs, see Figure 2b, shows a separation yield of 83.3%. The temporal evolution of the charge separation process and, in particular, hot and cold pathways were investigated in detail in ref 31. Here, our focus is on the thermodynamic quantities characterizing charge separation.

Figure 2c shows F^{st} and F^{eq} as a function of the intrapair distance relative to the smallest intrapair distance r_0 of all CT states. The free energy and the energy are smallest at close intrapair distances. The one-dimensional organic bilayer model only shows very few CT states at short distances of $r \leq 10$ nm, which are all strongly bound; see Figure 2a. The energy at equilibrium, E^{eq}, increases at short intrapair distances up to a value of 180 meV and only increases slightly up to 220 meV for distances beyond $r - r_0 \geq 10$ nm. F^{eq} shows a similar trend, while being up to 70 meV below E^{eq}. The difference is due to entropy contribution, which increases by 50−70 meV and shows minor fluctuations with the intrapair distance. At the steady state, the thermodynamic quantities show significant deviations from equilibrium. F^{st} increases up to 450 meV at $r - r_0 \approx 20$ nm and remains roughly constant for larger distances. The energy of occupied states even reaches values of 600 meV. In addition, the Gibbs entropy S^{st} shows 2−3 times the value of S^{eq}. Especially, a large slope in S^{st} for intrapair distances below 20 nm can be observed, which was shown to be highly desirable for electron−hole pairs to overcome their mutual Coulomb attraction.[18]

By considering equilibrated electron−hole pairs, one imposes an instant thermalization of electron−hole pairs at each time and every position. This, however, is a strong assumption, as highlighted by the stationary distributions. Our model shows that the thermodynamic quantities are not well-captured by the equilibrium assumption, which further suggests that photogenerated electron−hole pairs propagate through nonequilibrated CT states of higher energy and reach contact states before an equilibration in the density of states (DOS) can occur. This explains the significantly higher value in Gibbs entropy, as more CT states are available at higher energies with respect to tail states, which consequently increases the chance for charge separation. In realistic three-

https://doi.org/10.1021/acs.jpclett.1c01817
J. Phys. Chem. Lett. 2021, 12, 6389−6397

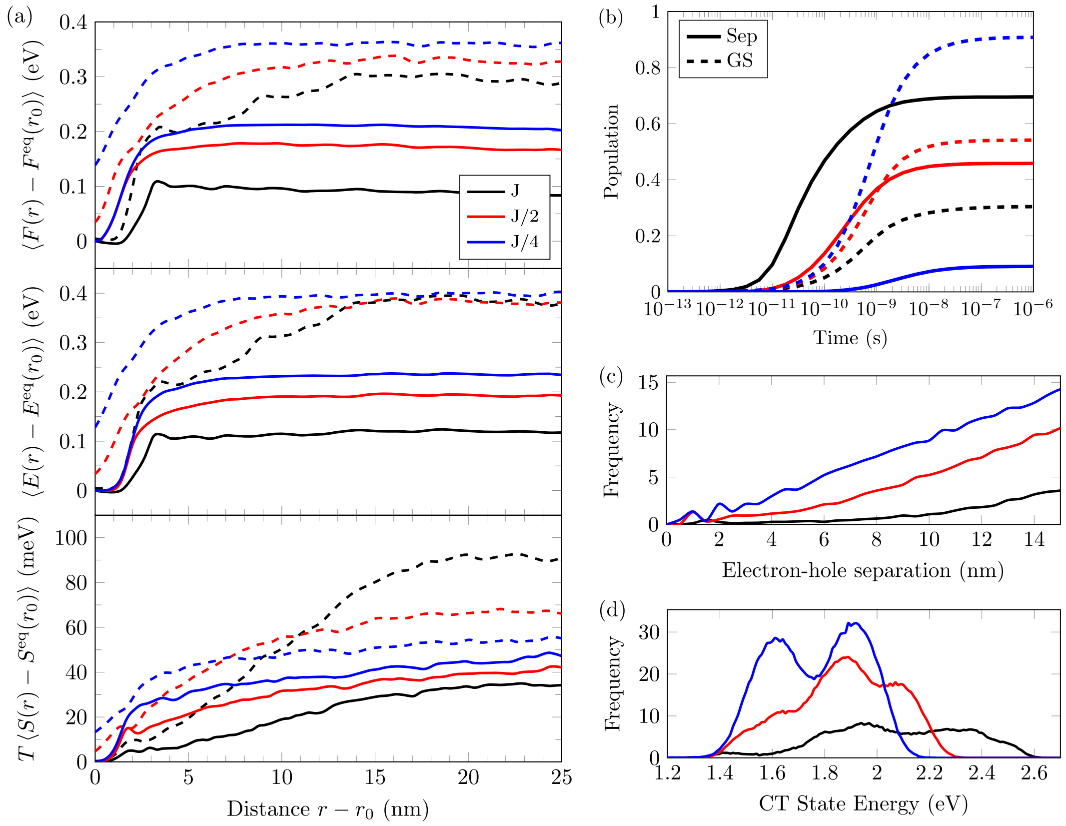

Figure 4. (a) Distance dependence of the free energy $F(r)$, energy $E(r)$, and entropy contribution $TS(r)$ for different coupling integrals: J (black), $J/2$ (red), and $J/4$ (blue). The $\langle\cdot\rangle$ labels the ensemble average over 256 configurations. r_0 gives the smallest distance of CT states in each configuration. Solid and dashed curves present the equilibrium and stationary quantities, respectively. All curves are normalized to the equilibrium value (superscript eq) at the distance r_0. (b) Time dependence of the separation yield (solid line) and the recombined states (dashed line). (c) Frequency of electron−hole separation and (d) of state energy of CT states with electron participation ratio PR ≤ 3 mimicking localized CT states. All curves in (a−d) show averages across 256 configurations.

dimensional (3D) systems, the entropy may reach even higher values and may dominate the energy contribution.[18,21,22]

We now study the role of the energetic disorder σ on the thermodynamic quantities for $\sigma \in \{50$ meV, 100 meV, 150 meV$\}$. For each σ, we take an ensemble average over 256 configurations to gain a reliable statistics. Figure 3a shows the thermodynamic quantities in the equilibrium and in the steady-state as a function of the intrapair distance $r - r_0$. First, we analyze the equilibrium quantities. F^{eq} decreases strongly with increased σ. For $\sigma \geq 100$ meV, F^{eq} even decreases with increased intrapair distance r as reported by Hood and Kassal.[19] The decrease in free energy with σ is mainly caused by a decrease in the average energy of populated states during charge separation, showing a similar distance dependence as the free energy. The entropy contribution shows significant differences for different σ. At $\sigma = 50$ meV, TS^{eq} increases monotonously with intrapair distance and reaches 35 meV. For larger σ, TS^{eq} is significantly reduced and reaches values of only 20 meV (10 meV) at $\sigma = 100$ meV (150 meV). At a high disorder, the entropy contribution remains roughly constant for $r - r_0 \geq 5$ nm.

For a low σ of 50 meV, significant differences between F^{eq} and F^{st} are observable. F^{st}, computed from realistic populations of CT states, increases up to 300 meV at $r - r_0 = 15$ nm, while F_{eq} remains roughly constant for $r - r_0 \geq 3$ nm. The entropy contribution shows a large increase up to 90 meV, which explains the difference between the free energy and energy. For $\sigma \geq 100$ meV, E^{st} differs by less than 40 meV from F^{st} due to a low entropy contribution. At $\sigma = 150$ meV, the entropy stays constant (∼20 meV) within the considered region. Entropy contributions that do not change with distance have been observed for 1D systems without disorder,[18] but also for two-dimensional (2D) systems with large σ values.[19]

Figure 3b visualizes the time dependence of fully separated and of recombined states for different σ. With increased σ, the separation yield decreases from 69.5% (σ = 50 meV) to 49.0% (σ = 100 meV) and 29.3% (σ = 150 meV). In addition, the time scale on which charge separation takes place increases by several orders of magnitude. At high σ, electron−hole pairs thermalize within the DOS and populate tail states. Equilibrated electron−hole pairs can only separate by propagation through low-energy states. The density of tail states, however, does not increase significantly with intrapair distance. A large σ value helps to initially separate charge carriers in space, while a low entropy slows further charge transport. The lack of available states leads to high recombination losses and can promote nongeminate recombination—which is neglected in this study—as a further limitation of charge separation.

To understand the efficient separation despite the large free energy barrier at a low σ, we analyze the delocalization of the CT states in terms of the participation ratio (PR, defined in eq S22, Supporting Information), which is a measure of the number of sites over which the electron (the hole) of the CT state delocalize. Figure 3c visualizes the PR distribution for different σ. At σ = 50 meV, a large spread in the PR with a high amount of delocalized CT states is observed. With a rising σ, the amount of strongly localized CT states increases significantly, and delocalized CT states of PR ≥ 5 vanish. All CT states with a low state energy show low PR values (see Figure S6, Supporting Information), that is, all energetically strongly bound CT states are strongly localized. The main difference between the configurations with different σ is that a large tail in the CT manifold of ~200−300 meV below the tail states at $\sigma = 50$ meV is observable (see Figure S7, Supporting Information). Several studies proposed that excitons can transform to delocalized CT states in the presence of a resonant coupling between donor excitons and delocalized CT states,[40,41] which can be assisted in the presence of substantial vibronic couplings.[42,43]

At $\sigma = 50$ meV, strongly bound electron−hole pairs with $r \leq 3$ nm face a large barrier in free energy (~300 meV), which makes it thermodynamically unfavorable to reach larger r values, while electron−hole pairs at distances larger than 3 nm see a strong reduction in the free energy barrier such that they need to overcome less than 100 meV in free energy to fully separate (see Figure 3a). Suppose the system starts in CT state with the smallest distance r_0, that is, in a strongly bound CT state. In that case, all the thermodynamic quantities during charge separation are well-described by the equilibrium populations; see Figure S2, Supporting Information. The chance that donor excitons transform to CT states of a large PR ratio, however, is high due to a large amount of delocalized CT states and the energetic resonance of XD and CT states (see Figure S7, Supporting Information). Thus, considering the transformation of donor excitons into CT states with a significant intrapair separation is crucial to understand the efficiency of the charge separation process.

One of the main observations from Figure 3 is that charge separation within OSCs with a high energetic disorder occurs close to equilibrium. To achieve efficient OSCs, however, typically low σ values are required.[44,45] High σ hinder the charge transport[46] and strongly reduce the attainable open-circuit voltage.[47,48] For high σ, electron−hole pairs lose energy while moving toward the contact states, matching previous reports.[49] In contrast, the rather delocalized electron−hole pairs at $\sigma = 50$ meV do not equilibrate and lose less energy before reaching the contact states. Our previous analysis (ref 31) showed that the separation goes via a cold pathway. The significant deviation in free energy for a low disorder, however, tells us that the separation of cold charge carriers does not happen in equilibrium and that charge pairs sample a relatively wide energy window before they eventually separate. Thus, we emphasize that charge separation in efficient OSCs occurs out of equilibrium. Thermodynamically, charge separation is favored in systems of a large energetic disorder. The kinetics of the charge carriers, however, is too slow to compete with charge recombination. An efficient separation of delocalized CT states in systems of low energetic disorder seems thermodynamically not favored, while their kinetics show a sufficient separation.

Now, we study the role of delocalization on the free energy; see Figure 4a. We increase charge localization by scaling all transfer integrals $J^{c/v}_{A/D,0/1}$ (see Figure 1a) with 1/2 and 1/4. According to both descriptions, the free energy increases with localization. Again, the energy follows the free energy closely. For $J/2$ and $J/4$, reduced separation yields of 45.9% and 9.1%, respectively, are observed (see Figure 4b). This agrees with the increase in the free energy and energy barrier with a larger localization. Interestingly, F^{st} deviates strongly from equilibrium for $J/2$ and $J/4$. At large distances, E^{st} approaches the same value of ~380 meV for different localization. In contrast, significant differences in E^{st} are observed for short distances; strongly localized electron−hole pairs occupy states with an energy of 130 meV (40 meV) above the equilibrium for $J/4$ ($J/2$).

The occupation of electron−hole states at the interface determines the measured emission spectra by electro- and photoluminescence studies of donor−acceptor blends, which are frequently related to the open-circuit voltage in OSCs.[50,51] Our results show that, especially for a strong localization, nonequilibrium state occupations of electron−hole pairs at the interface need to be considered. For a large localization, the probability of donor excitons transforming to a CT state with a small intrapair distance is higher because the number of such CT states strongly increases (see Figure 4c). The state population at the interface, following exciton dissociation to a CT state, is strongly impacted by the competition between thermalization dynamics and recombination. The significant deviation from equilibrium indicates that electron−hole pairs with small intrapair distances do not fully thermalize before recombination occurs, being in line with recent electroluminescence[24] and photoluminescence studies.[25] Strictly assuming equilibrated states may lead to a misinterpretation of experimental photo/electroluminescence data.

With an increased localization, the Gibbs entropy contribution deviates at short distances by up to 20 meV from equilibrium. Weak coupling integrals result in many CT states with small intrapair distances. Figure 4c,d visualizes the distribution of localized CT states, defined by the electron participation ratio of PR ≤ 3, in electron−hole separation and in CT state energy, respectively. For a large localization, the amount of localized CT states strongly increases for all intrapair distances. Especially at the interface, the amount of localized CT states is significantly higher than for the reference configuration. The distribution in energy (Figure 4d and Figure S10, Supporting Information, for individual states) of localized CT states shows a large spread, which can explain the deviation of F^{st} from equilibrium predictions. S^{st} differs from the equilibrium values as electron−hole pairs tend to recombine before thermalization is completed. Interestingly, S^{st} at short distances is roughly equal for different localizations (see Figure S3, Supporting Information). At a larger distance, the entropy increases more strongly with larger delocalizations. For $J/4$, the S^{st} value remains nearly constant, indicating that charge separation gets suppressed with an increased localization.

In contrast to previous theoretical studies,[23] our results emphasize that the free energy decreases with delocalization. In ref 23 the free energy was analyzed for electron−hole distances of less than 4 nm for a large energetic disorder of $\sigma \geq 100$ meV. An increase in coupling reduces the amount of electron−hole pairs with a small intrapair distance (cf. Figure 5 of ref 23), while only a few deep trap states remain. This may explain the predicted increase in free energy. However, efficient OSCs are characterized by long-range exciton separation, which can directly populate rather delocalized CT states of a large electron−hole distance and consequently reduce the relevance of strongly bound CT states, which comes closer to our model (see, e.g., Figure 4c).[2,4,7,12] Gluchowski et al.[23] further hypothesize that a potential improvement of the delocalization for charge separation may occur through nonequilibrium

https://doi.org/10.1021/acs.jpclett.1c01817
J. Phys. Chem. Lett. 2021, 12, 6389−6397

kinetic effects, which are particularly included within our model. This indicates that equilibrium thermodynamics results may provide potentially misleading conclusions and further underlines the relevance of our nonequilibrium thermodynamics analysis.

In conclusion, we have presented novel physical insights into the nonequilibrium thermodynamics of charge separation in OSCs by combining the phonon-assisted dynamics of electron−hole pairs within a 1D model Hamiltonian of an organic bilayer with the free energy based on the concept of stochastic thermodynamics. We derive thermodynamic quantities, in particular, the free energy, average energy, and entropy contributions of charge separation based on realistic steady-state populations for different energetic disorders and different localizations. In contrast to previous studies, the presented methodology accounts for the finite lifetime of CT states to provide more realistic thermodynamic quantities. Our analysis reveals significant deviations from equilibrium in the free energy and Gibbs entropy for delocalized electron−hole pairs at a small energetic disorder, representing efficient OSCs. While previous studies showed that charge separation occurs via cold pathways, our nonequilibrium thermodynamic analysis reveals that the separation of cold charge carriers in efficient OSCs proceeds out of the equilibrium. In systems of large energetic disorder, steady-state occupations of electron−hole pair states can be well-described as equilibrated. Furthermore, localized electron−hole pairs with small intrapair distances exhibit a significant nonequilibrium distribution, explaining previous observations from photoluminescence measurements. Our results emphasize that both a large Gibbs entropy and delocalized CT states at the interface can support efficient separation, while a decrease with distance in the free energy does not necessarily correlate with an enhanced charge separation. Overall, we believe that this work provides both an important contribution to understanding the physics of charge separation in organic semiconductors and a novel theoretical approach allowing access to nonequilibrium thermodynamic properties.

■ ASSOCIATED CONTENT

Supporting Information

The Supporting Information is available free of charge at https://pubs.acs.org/doi/10.1021/acs.jpclett.1c01817.

> Description of the model Hamiltonian and of the transition rate derivation of the organic bilayer; model parameters used in computations; numerical solution procedure of the Master equation; sensitivity analysis on hyperparameter σ_b; analysis on state energies, electron−hole pair distances, and state delocalization (PDF)

■ AUTHOR INFORMATION

Corresponding Author

Alessio Gagliardi − *Department of Electrical and Computer Engineering, Technical University of Munich, 80333 Munich, Germany;* orcid.org/0000-0002-3322-2190;
Email: alessio.gagliardi@tum.de

Authors

Waldemar Kaiser − *Department of Electrical and Computer Engineering, Technical University of Munich, 80333 Munich, Germany;* orcid.org/0000-0001-9069-690X

Veljko Janković − *Institute of Physics Belgrade, University of Belgrade, 11080 Belgrade, Serbia;* orcid.org/0000-0002-0297-2167

Nenad Vukmirović − *Institute of Physics Belgrade, University of Belgrade, 11080 Belgrade, Serbia;* orcid.org/0000-0002-4101-1713

Complete contact information is available at:
https://pubs.acs.org/10.1021/acs.jpclett.1c01817

Notes

The authors declare no competing financial interest.

■ ACKNOWLEDGMENTS

W.K. and A.G. acknowledge the TUM International Graduate School of Science and Engineering and Germany's excellence cluster *e*-conversion by the German Research Foundation (Deutsche Forschungsgemeinschaft) for funding. N.V. and V.J. acknowledge funding by the Institute of Physics Belgrade, through the grant by the Ministry of Education, Science, and Technological Development of the Republic of Serbia. Numerical computations were partially performed on the PARADOX-IV supercomputing facility at the Scientific Computing Laboratory, National Center of Excellence for the Study of Complex Systems, Institute of Physics Belgrade.

■ REFERENCES

(1) Bässler, H.; Köhler, A. Hot or cold: how do charge transfer states at the donor−acceptor interface of an organic solar cell dissociate? *Phys. Chem. Chem. Phys.* **2015**, *17*, 28451−28462.

(2) Grancini, G.; Maiuri, M.; Fazzi, D.; Petrozza, A.; Egelhaaf, H.; Brida, D.; Cerullo, G.; Lanzani, G. Hot exciton dissociation in polymer solar cells. *Nat. Mater.* **2013**, *12*, 29.

(3) Jones, M. L.; Dyer, R.; Clarke, N.; Groves, C. Are hot charge transfer states the primary cause of efficient free-charge generation in polymer: fullerene organic photovoltaic devices? A kinetic Monte Carlo study. *Phys. Chem. Chem. Phys.* **2014**, *16*, 20310−20320.

(4) Bakulin, A. A.; Rao, A.; Pavelyev, V. G.; van Loosdrecht, P. H.; Pshenichnikov, M. S.; Niedzialek, D.; Cornil, J.; Beljonne, D.; Friend, R. H. The role of driving energy and delocalized states for charge separation in organic semiconductors. *Science* **2012**, *335*, 1340−1344.

(5) Vandewal, K.; et al. Efficient charge generation by relaxed charge-transfer states at organic interfaces. *Nat. Mater.* **2014**, *13*, 63−68.

(6) Armin, A.; Kassal, I.; Shaw, P. E.; Hambsch, M.; Stolterfoht, M.; Lyons, D. M.; Li, J.; Shi, Z.; Burn, P. L.; Meredith, P. Spectral Dependence of the Internal Quantum Efficiency of Organic Solar Cells: Effect of Charge Generation Pathways. *J. Am. Chem. Soc.* **2014**, *136*, 11465−11472.

(7) Kahle, F.-J.; Saller, C.; Olthof, S.; Li, C.; Lebert, J.; Weiß, S.; Herzig, E. M.; Hüttner, S.; Meerholz, K.; Strohriegl, P.; Köhler, A. Does Electron Delocalization Influence Charge Separation at Donor−Acceptor Interfaces in Organic Photovoltaic Cells? *J. Phys. Chem. C* **2018**, *122*, 21792−21802.

(8) Deibel, C.; Strobel, T.; Dyakonov, V. Origin of the efficient polaron-pair dissociation in polymer-fullerene blends. *Phys. Rev. Lett.* **2009**, *103*, 036402.

(9) Tscheuschner, S.; Bässler, H.; Huber, K.; Köhler, A. A Combined Theoretical and Experimental Study of Dissociation of Charge Transfer States at the Donor−Acceptor Interface of Organic Solar Cells. *J. Phys. Chem. B* **2015**, *119*, 10359−10371.

(10) Janković, V.; Vukmirović, N. Combination of Charge Delocalization and Disorder Enables Efficient Charge Separation at Photoexcited Organic Bilayers. *J. Phys. Chem. C* **2018**, *122*, 10343−10359.

(11) Athanasopoulos, S.; Bässler, H.; Köhler, A. Disorder vs Delocalization: Which Is More Advantageous for High-Efficiency Organic Solar Cells? *J. Phys. Chem. Lett.* **2019**, *10*, 7107−7112.

(12) Felekidis, N.; Melianas, A.; Kemerink, M. The Role of Delocalization and Excess Energy in the Quantum Efficiency of Organic Solar Cells and the Validity of Optical Reciprocity Relations. *J. Phys. Chem. Lett.* **2020**, *11*, 3563−3570.

(13) Athanasopoulos, S.; Schauer, F.; Nádaždy, V.; Weiß, M.; Kahle, F.-J.; Scherf, U.; Bässler, H.; Köhler, A. What is the binding energy of a charge transfer state in an organic solar cell? *Adv. Energy Mater.* **2019**, *9*, 1900814.

(14) Shi, L.; Lee, C. K.; Willard, A. P. The Enhancement of Interfacial Exciton Dissociation by Energetic Disorder Is a Non-equilibrium Effect. *ACS Cent. Sci.* **2017**, *3*, 1262−1270.

(15) Köhler, A.; Bässler, H. *Electronic processes in organic semiconductors: An introduction;* John Wiley & Sons, 2015.

(16) Kaiser, W.; Albes, T.; Gagliardi, A. Charge carrier mobility of disordered organic semiconductors with correlated energetic and spatial disorder. *Phys. Chem. Chem. Phys.* **2018**, *20*, 8897−8908.

(17) Albes, T.; Gagliardi, A. Influence of permittivity and energetic disorder on the spatial charge carrier distribution and recombination in organic bulk-heterojunctions. *Phys. Chem. Chem. Phys.* **2017**, *19*, 20974−20983.

(18) Gregg, B. A. Entropy of charge separation in organic photovoltaic cells: the benefit of higher dimensionality. *J. Phys. Chem. Lett.* **2011**, *2*, 3013−3015.

(19) Hood, S. N.; Kassal, I. Entropy and disorder enable charge separation in organic solar cells. *J. Phys. Chem. Lett.* **2016**, *7*, 4495−4500.

(20) Gao, F.; Tress, W.; Wang, J.; Inganäs, O. Temperature Dependence of Charge Carrier Generation in Organic Photovoltaics. *Phys. Rev. Lett.* **2015**, *114*, 128701.

(21) Clarke, T. M.; Durrant, J. R. Charge Photogeneration in Organic Solar Cells. *Chem. Rev.* **2010**, *110*, 6736−6767.

(22) Nayak, P. K.; Narasimhan, K. L.; Cahen, D. Separating Charges at Organic Interfaces: Effects of Disorder, Hot States, and Electric Field. *J. Phys. Chem. Lett.* **2013**, *4*, 1707−1717.

(23) Gluchowski, A.; Gray, K. L.; Hood, S. N.; Kassal, I. Increases in the Charge Separation Barrier in Organic Solar Cells Due to Delocalization. *J. Phys. Chem. Lett.* **2018**, *9*, 1359−1364.

(24) Melianas, A.; Felekidis, N.; Puttisong, Y.; Meskers, S. C.; Inganäs, O.; Chen, W. M.; Kemerink, M. Nonequilibrium site distribution governs charge-transfer electroluminescence at disordered organic heterointerfaces. *Proc. Natl. Acad. Sci. U. S. A.* **2019**, *116*, 23416−23425.

(25) Brigeman, A.; Fusella, M.; Rand, B. P.; Giebink, N. Nonthermal site occupation at the donor-acceptor interface of organic solar cells. *Phys. Rev. Appl.* **2018**, *10*, 034034.

(26) Giazitzidis, P.; Argyrakis, P.; Bisquert, J.; Vikhrenko, V. S. Charge separation in organic photovoltaic cells. *Org. Electron.* **2014**, *15*, 1043−1049.

(27) Lankevich, V.; Bittner, E. R. Relating free energy and open-circuit voltage to disorder in organic photovoltaic systems. *J. Chem. Phys.* **2018**, *149*, 244123.

(28) Kawashima, E.; Fujii, M.; Yamashita, K. Entropy promotes charge separation in bulk heterojunction organic photovoltaics. *J. Photochem. Photobiol., A* **2019**, *382*, 111875.

(29) Van den Broeck, C.; Esposito, M. Ensemble and trajectory thermodynamics: A brief introduction. *Phys. A* **2015**, *418*, 6−16.

(30) Seifert, U. Stochastic thermodynamics, fluctuation theorems and molecular machines. *Rep. Prog. Phys.* **2012**, *75*, 126001.

(31) Janković, V.; Vukmirović, N. Energy−Temporal Pathways of Free-Charge Formation at Organic Bilayers: Competition of Delocalization, Disorder, and Polaronic Effects. *J. Phys. Chem. C* **2020**, *124*, 4378−4392.

(32) Rao, R.; Esposito, M. Nonequilibrium thermodynamics of chemical reaction networks: wisdom from stochastic thermodynamics. *Phys. Rev. X* **2016**, *6*, 041064.

(33) Leonard, T.; Lander, B.; Seifert, U.; Speck, T. Stochastic thermodynamics of fluctuating density fields: non-equilibrium free energy differences under coarse-graining. *J. Chem. Phys.* **2013**, *139*, 204109.

(34) Esposito, M.; Lindenberg, K.; Van den Broeck, C. Thermoelectric efficiency at maximum power in a quantum dot. *Europhys. Lett.* **2009**, *85*, 60010.

(35) Esposito, M.; Kawai, R.; Lindenberg, K.; Van den Broeck, C. Finite-time thermodynamics for a single-level quantum dot. *Europhys. Lett.* **2010**, *89*, 20003.

(36) Ajisaka, S.; Žunkovič, B.; Dubi, Y. The molecular photo-cell: Quantum transport and energy conversion at strong non-equilibrium. *Sci. Rep.* **2015**, *5*, 1−6.

(37) Nemati Aram, T.; Anghel-Vasilescu, P.; Asgari, A.; Ernzerhof, M.; Mayou, D. Modeling of molecular photocells: Application to two-level photovoltaic system with electron-hole interaction. *J. Chem. Phys.* **2016**, *145*, 124116.

(38) Aram, T. N.; Asgari, A.; Ernzerhof, M.; Quémerais, P.; Mayou, D. Quantum modeling of two-level photovoltaic systems. *EPJ Photovoltaics* **2017**, *8*, 85503.

(39) Qian, H. Relative entropy: Free energy associated with equilibrium fluctuations and nonequilibrium deviations. *Phys. Rev. E: Stat. Phys., Plasmas, Fluids, Relat. Interdiscip. Top.* **2001**, *63*, 042103.

(40) Savoie, B. M.; Rao, A.; Bakulin, A. A.; Gelinas, S.; Movaghar, B.; Friend, R. H.; Marks, T. J.; Ratner, M. A. Unequal partnership: Asymmetric roles of polymeric donor and fullerene acceptor in generating free charge. *J. Am. Chem. Soc.* **2014**, *136*, 2876−2884.

(41) Caruso, D.; Troisi, A. Long-range exciton dissociation in organic solar cells. *Proc. Natl. Acad. Sci. U. S. A.* **2012**, *109*, 13498−13502.

(42) Tamura, H.; Burghardt, I. Ultrafast charge separation in organic photovoltaics enhanced by charge delocalization and vibronically hot exciton dissociation. *J. Am. Chem. Soc.* **2013**, *135*, 16364−16367.

(43) Yao, Y.; Xie, X.; Ma, H. Ultrafast long-range charge separation in organic photovoltaics: promotion by off-diagonal vibronic couplings and entropy increase. *J. Phys. Chem. Lett.* **2016**, *7*, 4830−4835.

(44) Wu, J.; Lee, J.; Chin, Y.-C.; Yao, H.; Cha, H.; Luke, J.; Hou, J.; Kim, J.-S.; Durrant, J. R. Exceptionally low charge trapping enables highly efficient organic bulk heterojunction solar cells. *Energy Environ. Sci.* **2020**, *13*, 2422−2430.

(45) Liu, S.; Yuan, J.; Deng, W.; Luo, M.; Xie, Y.; Liang, Q.; Zou, Y.; He, Z.; Wu, H.; Cao, Y. High-efficiency organic solar cells with low non-radiative recombination loss and low energetic disorder. *Nat. Photonics* **2020**, *14*, 300−305.

(46) Pasveer, W.; Cottaar, J.; Tanase, C.; Coehoorn, R.; Bobbert, P.; Blom, P.; De Leeuw, D.; Michels, M. Unified description of charge-carrier mobilities in disordered semiconducting polymers. *Phys. Rev. Lett.* **2005**, *94*, 206601.

(47) Blakesley, J. C.; Neher, D. Relationship between energetic disorder and open-circuit voltage in bulk heterojunction organic solar cells. *Phys. Rev. B: Condens. Matter Mater. Phys.* **2011**, *84*, 075210.

(48) Kaiser, W.; Gagliardi, A. Kinetic Monte Carlo Study of the Role of the Energetic Disorder on the Open-Circuit Voltage in Polymer/Fullerene Solar Cells. *J. Phys. Chem. Lett.* **2019**, *10*, 6097−6104.

(49) Melianas, A.; Etzold, F.; Savenije, T. J.; Laquai, F.; Inganäs, O.; Kemerink, M. Photo-generated carriers lose energy during extraction from polymer-fullerene solar cells. *Nat. Commun.* **2015**, *6*, 1−8.

(50) Vandewal, K.; Tvingstedt, K.; Gadisa, A.; Inganäs, O.; Manca, J. V. Relating the open-circuit voltage to interface molecular properties of donor: acceptor bulk heterojunction solar cells. *Phys. Rev. B: Condens. Matter Mater. Phys.* **2010**, *81*, 125204.

(51) Rau, U. Reciprocity relation between photovoltaic quantum efficiency and electroluminescent emission of solar cells. *Phys. Rev. B: Condens. Matter Mater. Phys.* **2007**, *76*, 085303.

https://doi.org/10.1021/acs.jpclett.1c01817
J. Phys. Chem. Lett. 2021, 12, 6389−6397